EVALUATION OF TEMPERATURE DISTRIBUTION AND FLUID FLOW IN FUSION WELDING PROCESSES

Ass. Prof. Dr. Ihsan Y. Hussain
Mech. Engr. Dep.
College of Engr.
University of Baghdad
Baghdad – Iraq

Salah Sabeeh Abed - AlKareem
Al-Tahreer Institute
Ministry of Labor and Social Affairs
Baghdad – Iraq

ABSTRACT

A theoretical study of heat transfer and fluid flow phenomena in welding process has been carried out in the present work. The study involved the numerical solution of the transient Navier-Stokes and Energy equations of the weld pool region by using Finite Difference Method. The electromagnetic force field and buoyancy were included in the formulation The stream-vorticity formulation was used in the mathematical model. The numerical solution is capable of calculating the vorticity, stream function, velocity, temperature, and the interface movement of the weld pool in Gas Metal Arc Welding (GMAW). The model can be used to solve the Gas Tungesten Arc Welding (GTAW) problem. A numerical calculations algorithm was developed to carry out the numerical solution. The numerical results showed that the finger penetration phenomena occurs in the Gas Metal Arc weld is adequately explained through the application of the model. It is found that the frequency of spray transfer is a dominant factor in addition to shape of the weld pool geometry. A verification of numerical results was made through a comparison with a previous work, the agreement was good, confirming the capability and reliability of the proposed numerical algorithm in calculating fluid flow and heat transfer in Gas Metal Arc weld pools.

الخلاصة

في هذا البحث ، تمت دراسة انتقال الحرارة وجريان المائع في عمليات اللحام ألانصهاري نظرياً ، تضمنت الدراسة النظرية الحل العددي للمنظومة العابرة (غير المستقرة) لمعادلة الزخم والطاقة لمنطقة بركة اللحام (منطقة الطور المنصهر) باستخدام طريقة الفروق المحددة. تضمنت الصياغة قوة المجال الكهرومغناطيسي وقوة الطفو وتم استخدام صياغة الدوامية ودالة الانسياب في النمذجة الرياضية . أمكانية الحل العددي تتضمن حساب الدوامية ، دالة الانسياب ، السرعة ، درجة الحرارة والسطح البيني المتحرك لمنطقة اللحام بطريقة لحام القوس الكهربائي المعدني باستعمال غطاء غازي . هذا النموذج نستطيع استخدامه لحل المسألة بطريقة لحام القوس الكهربائي بقطب التنكستن باستعمال الغاز الواقي . تم التوصل لبرنامج حسابات عددية لتنفيذ الحل العددي . أظهرت النتائج العددية بأن ظاهرة التغلغل الإصبعي التي تحدث في طريقة لحام القوس الكهربائي المعدني باستعمال غطاء غازي وافية بالغرض للتوضيح من خلال التطبيق في النموذج المعمول به . لقد وجدنا بــأن مقدار أنتقال الرش الترددي هو العامل السائد بجانب الشكل الهندسي المستخرج لبركة اللحام . تمت مقارنة النتائج العددية التي تم إنجازها مع البحوث السابقة . التوافق بين النتائج جيد ويؤكد أمكانية وموثوقية الخطوات العددية المقترحة في حساب جريان المائع وانتقال الحرارة بطريقة لحام القوس الكهربائي المعدني باستعمال غطاء غازي في بركة اللحام .

KEY WORDS : Heat Transfer, Fluid Flow, Electromagnetic Force, Weld Pool, Numerical Solution

INTRODUCTION

The heat and fluid flow in the weld pool can significantly influence the pool geometry and the temperature gradients. A detailed knowledge of the temperature filed and thermally induced flow in a weld pool is important in understanding the phenomena and in development of improved welding techniques, and numerical simulations offer the possibility of avoiding this difficulty and provide a better quantitative description of the coupled solution behavior. If we consider a molten weld pool resulting from an applied surface temperature or heat flux, the thermal gradients induce buoyancy forces in the weld pool that tend to cause fluid flow. It is of considerable practical interest to understand quantitatively the heat and fluid flow phenomena in weld pool, because both the velocity and temperature distributions of molten metal affect the weld pool geometry, microstructure, and mechanical properties of the weld produced. Inherent to the welding process is the formation of a pool of molten metal directly below the heat source. The shape of this molten pool is influenced by the flow of both heat and metal, with melting occurring ahead of the heat source and solidification behind it. Fluid flow in weld pool can strongly affect the quality of the resultant weld. Variations in the weld characteristics, which are likely to occur from changes in the weld pool fluid flow are weld penetration, undercutting, surface smoothness segregation pattern, gas porosity and solidification structure, **(Gukan and Sundararajan. 2001)**, see **Fig.1**. The problem was investigated in literatures with different approaches, **(Oreper and Szekely.1987)** developed a general mathematical statement to describe the transient weld pool development. In the formulation, axi-symmetric systems are considered and allowance is made for buoyancy, surface tension, and electromagnetic forces. **(Tsao and Wu.1988)** developed a mathematical model to evaluate the effect of the electromagnetic force field, the velocity field and the temperature field in a Gas Metal Arc (GMA) weld pool. **(Tsai and Kou. 1990)** studied the convection flow induced by the electromagnetic force in the weld pool during gas tungsten arc welding. In order to accurately describe the boundary conditions, **(Kim and Na. 1994)** developed a computer simulation of three dimensional heat transfer and fluid flow in Gas Metal Arc (GMA) welding by considering the three driving forces for weld-pool convection. **(Gukan, et. al. 2001)** developed a systematic study of a two dimensional model to analyze the role of convection in the stationary (GTA) welds to analyze the behavior of weld pool convection and its effect on the weld geometry.

The present work represents the beginning of a new research line in Iraq that aims to investigate the thermal and fluid flow phenomena associated with welding process. A computational study of fluid flow and heat transfer phenomena occurred in the weld pool. The simulation covers the molten phase, the two phase and the solid phase region.

MATHEMATICAL MODEL

Fig.2 shows a diagram of a Gas Metal Arc (GMA) liquid pool and the cylindrical coordinate system chosen for analysis. Velocities along the radial and axial directions are expressed as U and V, respectively. A spatially distributed heat flux, q(r), and current flux, j(r), fall on the free surface at (Z = 0), which is the surface of the workpiece, the energy exchange between the spray droplets and molten pool is ΔH.As shown in **Fig.2**, let U=U(r,z) and V=V(r,z) denote the velocity components in the radial r and axial z directions, respectively. The unsteady-state continuity, momentum and energy equation of the incompressible fluid in the molten pool is **(Salah. 2005)** ;

$$\frac{1}{r}\frac{\partial}{\partial r}(rU)+\frac{\partial}{\partial z}(V)=0 \tag{1}$$

$$\rho\left(\frac{\partial U}{\partial t}+U\frac{\partial U}{\partial r}+V\frac{\partial U}{\partial z}\right)=F_r-\frac{1}{\rho}\frac{\partial p}{\partial r}+\mu\left[\frac{\partial}{\partial r}\left(\frac{1}{r}\frac{\partial}{\partial r}(rU)\right)+\frac{\partial^2 U}{\partial z^2}\right] \tag{2}$$

$$\rho\left(\frac{\partial V}{\partial t}+U\frac{\partial V}{\partial r}+V\frac{\partial V}{\partial z}\right)=F_z-\frac{1}{\rho}\frac{\partial p}{\partial z}+\mu\left[\frac{1}{r}\frac{\partial}{\partial r}\left(r\frac{\partial V}{\partial r}\right)+\frac{\partial^2 V}{\partial z^2}\right] \tag{3}$$

$$\left(\frac{\partial T}{\partial t}+U\frac{\partial T}{\partial r}+V\frac{\partial T}{\partial z}\right)=\alpha\left[\frac{\partial^2 T}{\partial^2 r}+\frac{1}{r}\frac{\partial T}{\partial r}+\frac{\partial^2 T}{\partial^2 z}\right]+\Delta H/\rho C_p \tag{4}$$

Using the vorticity transport formulation **(Salah 2005)**, it can be shown that ;

$$\frac{\partial \omega}{\partial t}+\frac{\partial(U\omega)}{\partial r}+\frac{\partial(V\omega)}{\partial z}=\upsilon\left[\frac{\partial}{\partial r}\left(\frac{1}{r}\frac{\partial(r\omega)}{\partial r}\right)+\frac{\partial^2\omega}{\partial z^2}\right]+g\beta\frac{\partial T}{\partial r}+\nabla\times\left(\bar{j}\times\bar{B}\right) \tag{5}$$

The stream function equation is ;

$$\frac{\partial}{\partial z}\left(\frac{1}{r}\frac{\partial\psi}{\partial z}\right)+\frac{\partial}{\partial r}\left(\frac{1}{r}\frac{\partial\psi}{\partial r}\right)=-\omega=\nabla^2\psi \tag{6}$$

The temperature equation in the conservative form is ;

$$\frac{\partial T}{\partial t}+\frac{1}{r}\frac{\partial(rUT)}{\partial r}+\frac{\partial(VT)}{\partial z}=\alpha\left[\frac{\partial^2 T}{\partial r^2}+\frac{1}{r}\frac{\partial T}{\partial r}+\frac{\partial^2 T}{\partial z^2}+\frac{\Delta H}{\rho C_p}\right] \tag{7}$$

The electromagnetic force term in **equ.(5)** is **(Tsao and Wu 1988)** ;

$$\nabla\times\left(\bar{j}\times\bar{B}\right)=\frac{C_o\mu_o l^2}{2\pi^2 L r^3}\left[1-\exp\left(-\frac{r^2}{2\sigma_j^2}\right)\right]^2\left(1-\frac{z}{L}\right) \tag{8}$$

and the energy exchange (ΔH) is ;

$$\Delta H=(2.28 f\, e^{-C_1 r^2}) \tag{9}$$

Initial and Boundary Conditions Representations

The initial conditions used to solve temperature, vorticity and stream function equations are ;
$T_{i,j}=w_{i,j}=\psi_{i,j}=V_{i,j}=0$ at t=0
The boundary conditions used are given in **Fig.3** .

NUMERICAL SOLUTION

The governing equations mentioned above were solved numerically by using the FDM. A grid arrangement was generated with the notation of **Fig.4**. The temperature of each grid point in weldment is compared with the melting temperature T_m. Once the liquid region emerges, the fluid flow and heat transfer in the weld pool and the heat conduction out of the molten pool are calculated.

The nodal equation at i=1 ; $1\leq j\leq M$

$$\therefore T'_{1,j}=(a_1+a_2)T_{2,j}+a_3 T_{1,j}+a_4 T_{1,j-1}+a_5 T_{1,j+1}+B(i) \tag{10}$$

The nodal equation at i=1 ; j =1

$$T'_{1,1}=(a_1+a_2)T_{2,1}+a_3 T_{1,1}+(a_4+a_5)T_{1,2}+a_4\frac{2\Delta z}{K}q(i)+B(i) \tag{11}$$

The nodal equation at $2\leq i\leq R/\Delta r+1$ (i.e r=R)

$$T'_{i,1}=a_1 T_{i-1,1}+a_2 T_{i+1,1}+a_3 T_{i,1}+(a_4+a_5)T_{i,2}+a_4\frac{2\Delta z}{K}q(i)+B(i) \tag{12}$$

At i=1 ; j =1

$$T'(i,j) = (1 - 4*k*dt/(row*cp*dr^2) - 2*us*dt/dr - 2*vs*dt/dr)*T(i,j) +$$
$$(2*k*dt/(row*cp*dr^2) + 2*us*dt/dr)*T(i+1;j) + \ldots\ldots$$
$$(2*k*dt/(row*cp*dr^2) + 2*vs*dt/dr)*T(i,j+1) +$$
$$2*a1ph*q(i)*dt/(row*cp*dr^2) + dH(i)*dt/(row*cp) \; ; \ldots \hspace{2cm} (13)$$

At i=1 ; j =M

$$T'(i,j) = (1 - 4*k*dt/(row*cp*dr^2) - 2*h*dt/(row*cp*dr))*T(i,j) +$$
$$(2*k*dt/(row*cp*dr^2))*T(i+1,j) + \ldots (2*k*dt/(row*cp*dr^2))*T(i,j-1)$$
$$+ (2*h*dt/(row*cp*dr))*Ta \; ; \ldots \hspace{2cm} (14)$$

At i=1 ; JFL < j < M

$$T'(i,j) = (1 - 4*k*dt/(row*cp*dr^2))*T(i,j) + (2*k*dt/(row*cp*dr^2))*T(i+1,j) + \ldots$$
$$(k*dt/(row*cp*dr^2))*T(i,j+1) + (k*dt/(row*cp*dr^2))*T(i,j-1) \; ; \ldots \hspace{2cm} (15)$$

At 1< i < N_q ; j=1

$$T'(i,j) = (1 - 4*k*dt/(row*cp*dr^2) - 2*us*dt/dr - 2*vs*dt/dr)*T(i,j) +$$
$$(k*dt/(row*cp*dr^2) + us*dt/dr)*T(i+1,j) + (k*dt/(row*cp*dr^2) +$$
$$us*dt/dr)*T(i-1,j) + \ldots (2*k*dt/(row*cp*dr^2) + 2*vs*dt/dr)*T(i,j+1) +$$
$$2*dt*q(i)*a1ph/(row*cp*dr^2) + dH(i)*dt/(row*cp) \; ; \ldots \hspace{2cm} (16)$$

At i=N_q ; j=1

$$T'(i,j) = (1 - 4*k*dt/(row*cp*dr^2) - 2*h*dt/(row*cp*dr) - us*dt/dr)*T(i,j)$$
$$+ (k*dt/(row*cp*dr^2))*T(i+1,j) + (k*dt/(row*cp*dr^2) + us*dt/dr)*T(i-1,j)$$
$$+ \ldots (2*k*dt/(row*cp*dr^2))*T(i,j+1) + 2*h*dt*Ta/(row*cp*dr) +$$
$$dH(i)*dt/(row*cp) \; ; \ldots \hspace{2cm} (17)$$

At i=N ; j=1

$$T'((i,j) = (1 - 4*k*dt/(row*cp*dr^2) - 4*h*dt/(row*cp*dr))*T(i,j) +$$
$$(2*k*dt/(row*cp*dr^2))*T(i,j+1) + (2*k*dt/(row*cp*dr^2))*T(i-1,j) +$$
$$(4*h*dt/(row*cp*dr))*Ta \; ; \ldots \hspace{2cm} (18)$$

At N_q < i < N ; j=1

$$T'(i,j) = (1 - 4*k*dt/(row*cp*dr^2) - 2*h*dt/(row*cp*dr))*T(i,j) +$$
$$(k*dt/(row*cp*dr^2))*T(i+1,j) + (k*dt/(row*cp*dr^2))*T(i-1,j) + \ldots$$
$$(2*k*dt/(row*cp*dr^2))*T(i,j+1) + (2*h*dt/(row*cp*dr))*Ta \; ; \ldots \hspace{2cm} (19)$$

At i=N ; j=M

$$T'(i, j) = (1 - 4*k*dt/(row*cp*dr^2) - 4*h*dt/(row*cp*dr))*T(i, j) +$$
$$(2*k*dt/(row*cp*dr^2))*T(i-1, j) + (2*k*dt/(row*cp*dr^2))*T(i, j-1) +$$
$$(4*h*dt/(row*cp*dr))*Ta ;... \tag{20}$$

At 1< i < N ; j=M

$$T'(i, j) = (1 - 4*k*dt/(row*cp*dr^2) - 2*h*dt/(row*cp*dr))*T(i, j) +$$
$$(k*dt/(row*cp*dr^2))*T(i+1, j) + (k*dt/(row*cp*dr^2))*T(i-1, j) +....$$
$$(2*k*dt/(row*cp*dr^2))*T(i, j-1) + (2*h*dt/(row*cp*dr))*Ta ;.... \tag{21}$$

At i = N ; 1< j < M

$$T'(i, j) = (1 - 4*k*dt/(row*cp*dr^2) - 2*h*dt/(row*cp*dr))*T(i, j) +$$
$$(2*k*dt/(row*cp*dr^2))*T(i-1, j) + (k*dt/(row*cp*dr^2))*T(i, j+1) +.....$$
$$(k*dt/(row*cp*dr^2))*T(i, j-1) + (2*h*dt/(row*cp*dr))*Ta ;..... \tag{22}$$

At 1< i < IFL (j) ; 1< i < IFL

$$T'(i, j) = (1 - 4*k*dt/(row*cp*dr^2))*T(i, j) + (k*dt/(row*cp*dr^2))*T(i+1, j)$$
$$+ (k*dt/(row*cp*dr^2))*T(i-1, j) +.....(k*dt/(row*cp*dr^2))*T(i, j+1) +$$
$$(k*dt/(row*cp*dr^2))*T(i, j-1) ;... \tag{23}$$

The temperature equation in weld pool ;

$$T'_{i,j} = aT_{i-1,j} + a_2 T_{i+1,j} + a_3 T_{i,j} + a_4 T_{i,j-1} + a_5 T_{i,j+1} + B \tag{24}$$

Where ;

$$a_1 = \frac{-\Delta t(U_b + |U_b|)\ (1-2i)}{4i\Delta r} + \frac{\alpha\Delta t(i - 0.5)}{i(\Delta r)^2}$$

$$a_2 = \frac{-\Delta t(U_f - |U_f|)(1+2i)}{4i\Delta r} + \frac{\alpha\Delta t(i + 0.5)}{i(\Delta r)^2}$$

$$a_3 = 1 - \Delta t\left(\frac{(U_f + |U_f|)(1+2i) + (U_b + |U_b|)(1-2i)}{4i\Delta r}\right).$$

$$\Delta t\left(\frac{(V_f + |V_f| - V_b + |V_b|)}{2\Delta z} + \frac{2\alpha}{(\Delta z)^2} + \frac{2\alpha}{(\Delta r)^2}\right) \tag{25}$$

$$a_4 = \frac{\Delta t(V_b + |V_b|)}{2\Delta z} + \frac{\alpha\Delta t}{(\Delta z)^2}$$

$$a_5 = \frac{-\Delta t(V_f + |V_f|)}{2\Delta z} + \frac{\alpha\Delta t}{(\Delta z)^2}$$

$$B = \Delta t(2.28\ fe^{-C_1(i\Delta r)^2})/\rho C_P$$

The electromagnetic force field in the vorticity equation ;

$$\nabla \times (\bar{J} \times \bar{B}) = \frac{C_o \mu_o I^2}{2\pi^2 L (i\Delta r)^3} \left[1 - \exp\left(-\frac{(i\Delta r)^2}{2\sigma_j^2} \right) \right]^2 \left(1 - \frac{j\Delta z}{L} \right) \tag{26}$$

$$\omega'_{i,j} = b_1 \omega_{i-1,j} + b_2 \omega_{i+1,j} + b_3 \omega_{i,j} + b_4 \omega_{i,j-1} + b_5 \omega_{i,j+1} + C \tag{27}$$

$$b_1 = \frac{\Delta t (U_b + |U_b|)}{2\Delta r} + \frac{\Delta t \upsilon (i - 0.5)}{i (\Delta r)^2}$$

$$b_2 = \frac{-\Delta t (U_f - |U_f|)}{2\Delta r} + \frac{\Delta t \upsilon (i + 0.5)}{i (\Delta r)^2}$$

$$b_3 = 1 - \Delta t \left(\frac{(U_f + |U_f| - U_b + |U_b|)}{2\Delta r} + \frac{(V_f + |V_f| - V_b + |V_b|)}{2\Delta z} \right)$$

$$- \Delta t \left(+ \frac{2\upsilon}{(\Delta z)^2} + \frac{2\upsilon}{(\Delta r)^2} + \frac{\upsilon}{(i\Delta r)^2} \right) \tag{28}$$

$$b_4 = \frac{\Delta t (V_b + |V_b|)}{2\Delta z} + \frac{\Delta t \upsilon}{(\Delta z)^2}$$

$$b_5 = \frac{-\Delta t (V_f + |V_f|)}{2\Delta z} + \frac{\Delta t \upsilon}{(\Delta z)^2}$$

$$C = \frac{\Delta t g \beta (T'_{i+1,j} - T'_{i-1,j})}{2\Delta r} + \frac{\Delta t C_o \mu_o I^2}{2\pi^2 L (i\Delta r^3)} \left[1 - \exp\left(-\frac{(i\Delta r)}{2\sigma_j^2} \right) \right]^2 \left(1 - \frac{j\Delta z}{L} \right)$$

The temperature equation at the centerline as ;

$$\frac{T_{0,j} - T_{0,j}}{\Delta t} + \frac{2T_{1,j}(Uf_0 - |Uf_0|) + 2T_{0,j}(Uf_0 + |Uf_0|)}{\Delta r} +$$

$$\frac{(Vf_0 - |Vf_0|)T_{0,j+1} + (Vf_0 - |Vf_0| - Vb_0 + |Vb_0|)T_{0,j}}{2\Delta z} - \frac{(Vb_0 + |Vb_0|)T_{0,j-1}}{2\Delta z} =$$

$$\alpha \left[\frac{4(T_{1,j} - T_{0,j})}{(\Delta r)^2} + \frac{T_{0,j+1} - 2T_{0,j} + T_{0,j-1}}{(\Delta z)^2} \right] + \frac{\Delta H}{\rho C_p} \tag{29}$$

Where ;

$$C_1 = \frac{4\alpha\Delta t}{(\Delta r)^2} - \frac{2\Delta t(Uf_0 - |Uf_0|)}{\Delta r}$$

$$C_2 = 1 - \Delta t\left[\frac{2(Uf_0 - |Uf_0|)}{\Delta r} + \frac{(Vf_0 + |Vf_0| - Vb_0 + |Vb_0|)}{2\Delta z} + \frac{4\alpha}{(\Delta r)^2} + \frac{2\alpha}{(\Delta z)^2}\right]$$

$$C_3 = \frac{-\Delta t(Vf_0 - |Vf_0|)}{2\Delta z} + \frac{\alpha\Delta t}{(\Delta z)^2}$$

$$C_4 = \frac{\Delta t(Vb_0 + |Vb_0|)}{2\Delta z} + \frac{\alpha\Delta t}{(\Delta z)^2}$$

$$C_5 = \frac{\Delta t\Delta H}{\rho C_p}$$

(30)

The vorticity equation at centerline ;

$$\omega'_{0,j} = D_1\omega_{1,j} + D_2\omega_{0,j} + D_3\omega_{0,j+1} + D_4\omega_{0,j-1} + D_5$$

(31)

Where ;

$$D_1 = \frac{-\Delta t(Uf_0 - |Uf_0|)}{2\Delta r} - \frac{\Delta t(Ub_0 + |Ub_0|)}{2\Delta r}$$

$$D_2 = 1 - \frac{\Delta t(Uf_0 + |Uf_0| - Ub_0 + |Ub_0|)}{2\Delta r} - \frac{\Delta t(Vf_0 + |Vf_0| - Vb_0 + |Vb_0|)}{2\Delta z} - \frac{2\nu\Delta t}{(\Delta r)^2} - \frac{2\nu\Delta t}{(\Delta z)^2}$$

$$D_3 = \frac{-\Delta t(Vf_0 - |Vf_0|)}{2\Delta z} + \frac{\nu\Delta t}{(\Delta z)^2}$$

$$D_4 = \frac{-\Delta t(Vb_0 - |Vb_0|)}{2\Delta z} + \frac{\nu\Delta t}{(\Delta z)^2}$$

$$D_5 = \frac{\Delta t C_0 \mu_0 I^2}{2\pi^2 L(i\Delta r)^3}\left[1 - \exp\frac{-(i\Delta r)^2}{2\sigma_j^2}\right]^2\left(1 - \frac{i\Delta z}{L}\right)$$

(32)

The stream function for the next iteration (m+1) ;

$$\psi_{i,j}^{(m+1)} = (1-\Omega)\psi_{i,j}^{(m)} + \frac{\Omega}{4}\left[i(\Delta r)^3\omega'i,j + \left(\psi_{i+1,j}^{(m)}\left(1-\frac{1}{i}\right) + \psi_{i-1,j}^{(m+1)}\left(1+\frac{1}{i}\right)\right)\right.$$
$$\left. + \left(\psi_{i,j+1}^{(m)} + \psi_{i,j-1}^{(m+1)}\right)\right]$$

(33)

From **(Petrovic and Stuper. 1996)** ;

$$\gamma = \left[\frac{\cos\frac{\pi}{(N_r-1)} + \left(\frac{\Delta r}{\Delta z}\right)^2\cos\frac{\pi}{(N_z-1)}}{1 + \left(\frac{\Delta r}{\Delta z}\right)^2}\right]^2$$

(34)

$$\Omega_{OPT} = \frac{2 - 2\sqrt{1-\gamma}}{\gamma} \tag{35}$$

The radial and vertical velocities ;

$$U_{i,j} = \frac{\left(\Psi_{i,j+1} - \Psi_{i,j-1}\right)}{i\Delta r\Delta z} \tag{36}$$

$$V_{i,j} = -\frac{\left(\Psi_{i+1,j} - \Psi_{i-1,j}\right)}{i(\Delta r)^2} \tag{37}$$

Calculation of the Vertical Velocity at Centerline from **(Chow.1979)** ;

$$V_{0,j} = \frac{-2\Psi_{1,j}}{i(\Delta r)^2} \tag{38}$$

RESULTS AND DISCUSSIONS

Fig.5 shows the computed isotherms and convection patterns in the pool of the weld to account for convection and temperature distribution in moving weld pools driven by buoyancy and electromagnetic forces at times (0.1, 0.3, 0.5 and 0.75 seconds). As time passes, the molten pool increases for MIG welding process. The deep penetration is observed in the figure. The liquidus temperature is 1440°C and the solidus 1000°C. **Fig.6** shows the computed stream function in the case of combined buoyancy and electromagnetically driven flow of the weld pool at times (0.1, 0.3, 0.5 and 0.75 seconds), respectively. As time passes, the molten pool increases. **Fig.7** shows a strong counterclockwise circulation pattern, with very high velocities, which is dominated by the combined effect of the buoyancy and electromagnetically driven flow components. The weld pool shape, involving deep penetration, is consistent with the circulation pattern, (0.1, 0.3, 0.5 and 0.75 seconds), and the large the weld pool. It is this transfer of additional heat from the metal droplets (ΔH) in the GMA process which plays a very important role in the formation of the finger penetration in the GMA welds. This phenomenon is not present in the GTAW process. **Figs.8 and 9** show the interface between the molten pool and the solid region at different times (0.1, 0.5, 0.75 and 1 seconds) respectively during MIG and TIG welding processes. A comparison between the calculated numerical results of the present work and the results of TSAO and Wu (1988) will be made for verification. Some results were selected in order to check the model. Figures (8) and (9) of the present work may be compared with **Figs 10 and 11** of **(TSAO and Wu 1988)** for GMA and TIG results. The comparison show good qualitative and quantitative agreement.

CONCLUSIONS

A numerical study of heat transfer and fluid flow phenomena in welding process has been carried out in the present work. The weld pool size in GMA welding increases at a faster rate at small times (0.1 – 0.3 Sec.) and the stream function at times 0.1 sec and 0.3 sec appear increasing in the (r) and (z) directions. Two circulation loops in the weld pool appears one near the free surface and the other in the bulk weld pool, the maximum velocity which occurs at the free surface. And the flow at the free surface is radially outward from the (z) axis to the pool boundary.
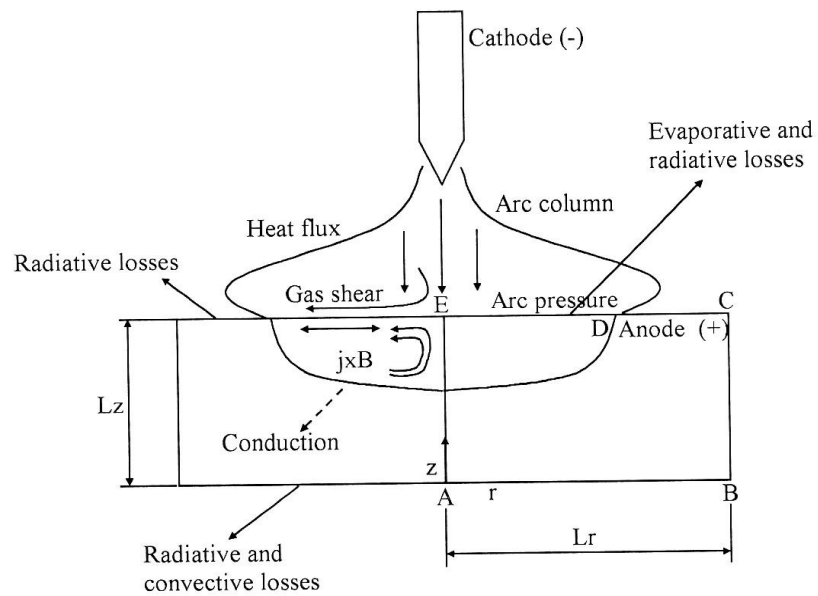
Fig. (1): Schematic Representation of Gas Tungsten arc Weld
Phenomena (Gukan and Sundararajan 2001).
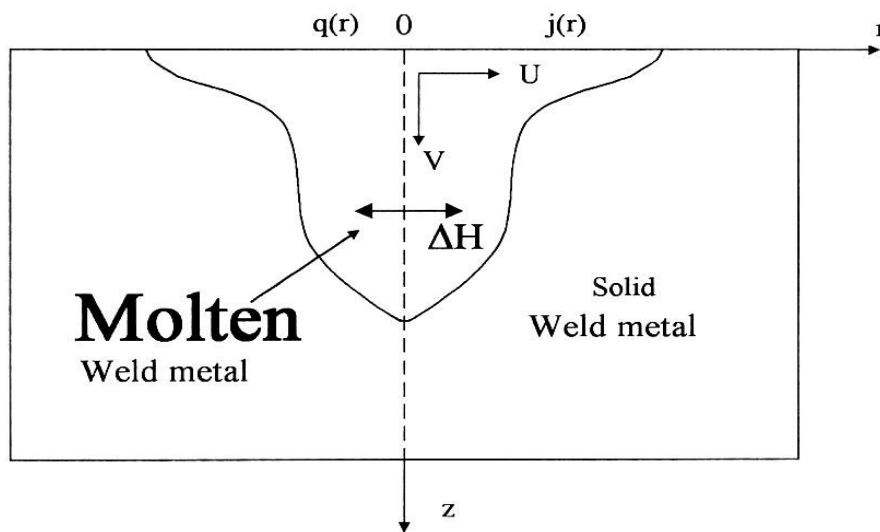
Fig. (2): Sketch the weldment of GMAW

$$\psi_{i,j} = 0$$

$$\mu\omega_{i,0} = (-\frac{\partial\sigma}{\partial T})(\frac{\partial T}{\partial r}) \mid_{i,0}$$

$$q_{(r)} = \frac{Q}{2\pi\sigma_q^2} \exp\left[\frac{-(i\Delta r)^2}{2\sigma_q^2}\right]$$

equ.(13)
equ.(11)

equ. (16)
equ.(12)

equ.(17)

equ. (18)

(1,1)

IFL

Nq

N

$r_{(i)}$

equ.(29)
equ.(31)
equ.(38)

equ.(24)
equ.(27)
equ.(33)
equ.(36)
equ.(37)

equ. (19)

$$\psi_{i,j} = 0$$

$$\frac{\partial}{\partial r}(\frac{\omega}{r}) \mid_{0,j} = 0$$

$$\psi_{i,j} = 0$$

$$T_{i,j} = T_m$$

equ.(10)

$$\frac{\partial T}{\partial r} \mid_{0,j} = 0$$

$$\frac{\partial\psi}{\partial r} = \frac{\partial\psi}{\partial Z} = 0$$

equ.(23)

equ. (22)

H

JFL

$$-K\frac{\partial T}{\partial r} \mid_{r=w} = h(T_{i,j} - Ta)$$

equ. (15)

equ. (20)

M

N , M

equ. (14)

W

equ. (21)

$$-K_s \frac{\partial T}{\partial Z} \mid_{Z=H} = h(T_{i,j} - Ta)$$

$Z_{(j)}$
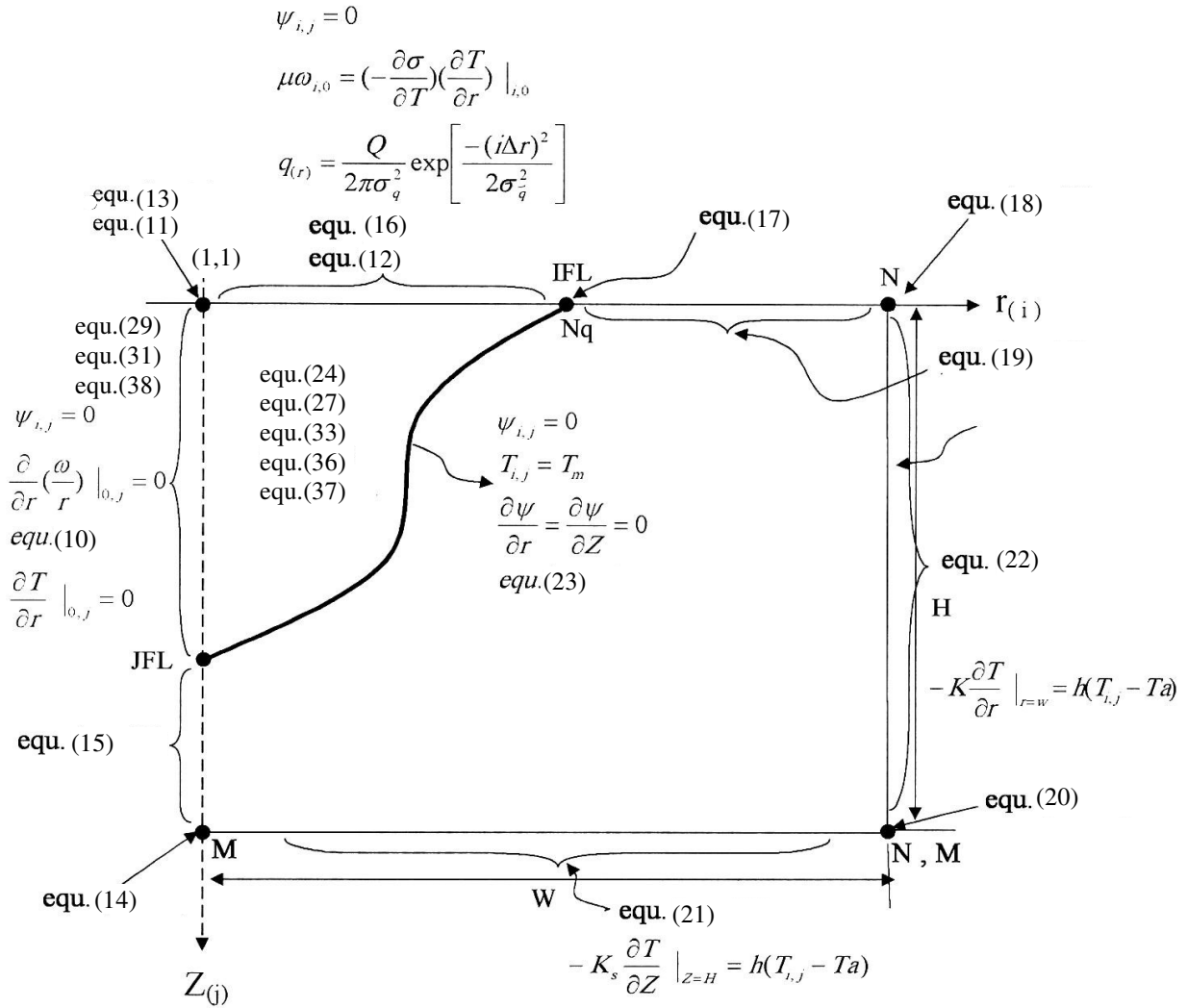
Fig.(3): Nodes Equations of the Numerical grid arrangement of weldment using temperature distribution , pool temperature distribution and boundary conditions used in calculations
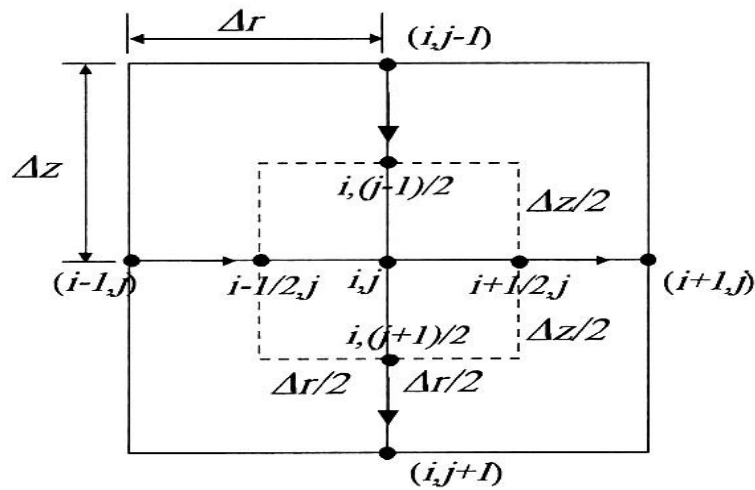
Fig. (4) The Nodal Points Used in Numerical Solution
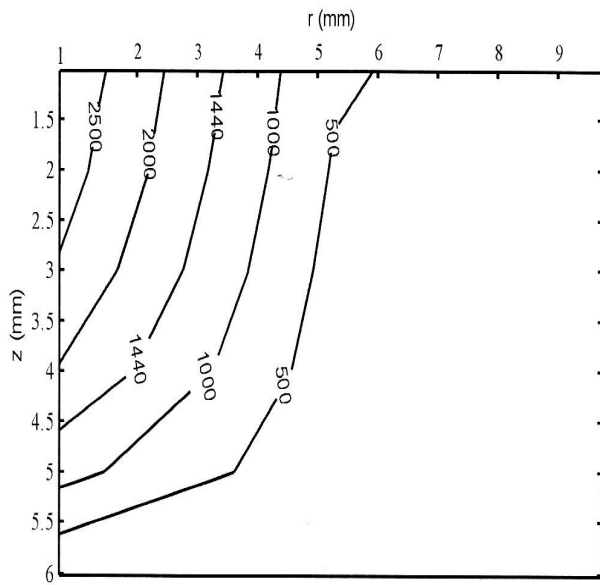
a. 0.1 sec
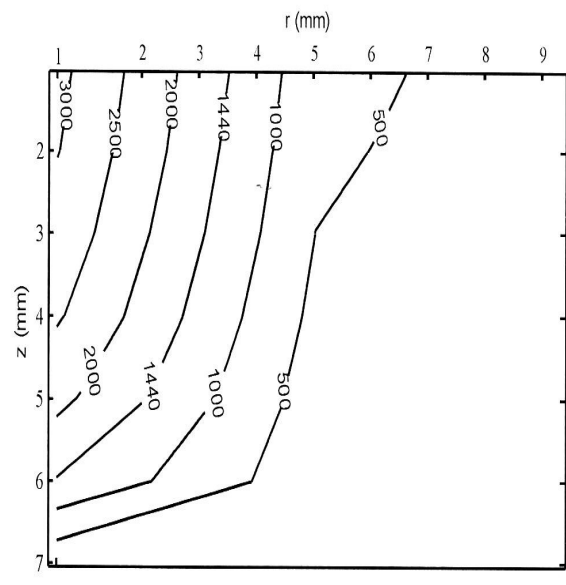
c. 0.5 sec
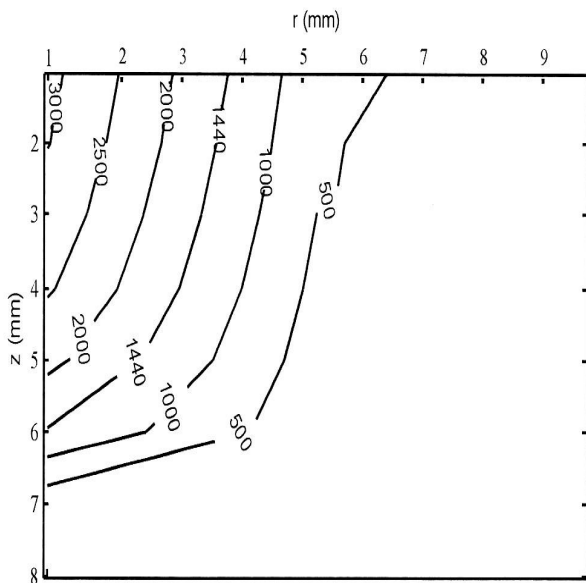
b. 0.3 sec
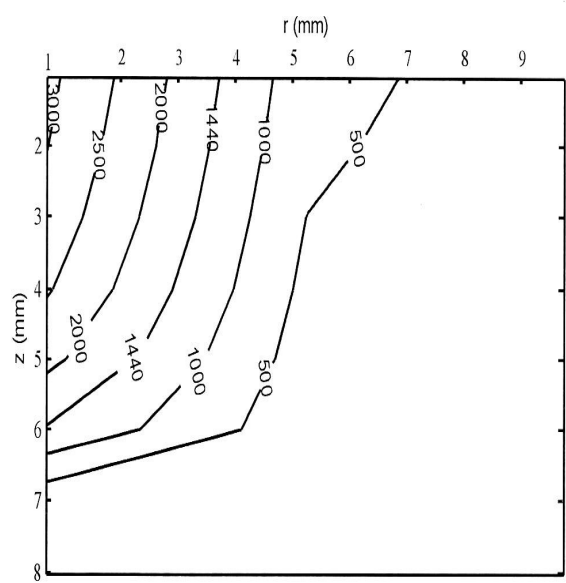
d. 0.7 sec

Fig. (5): Calculated Temperature Distribution at Different Times in GMA Weld Pool.
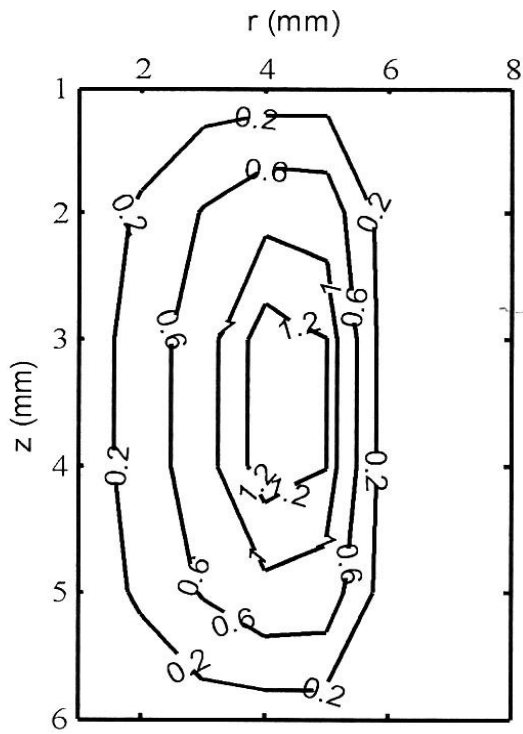
a. 0.1 sec
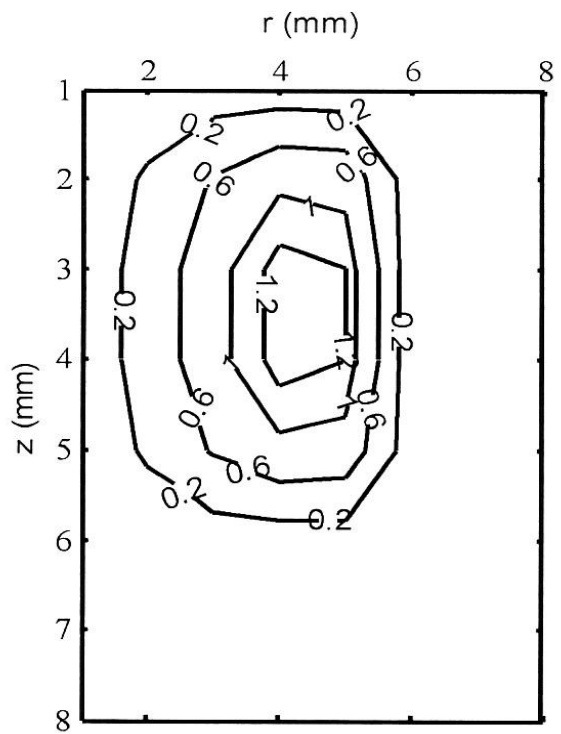
b. 0.3 sec
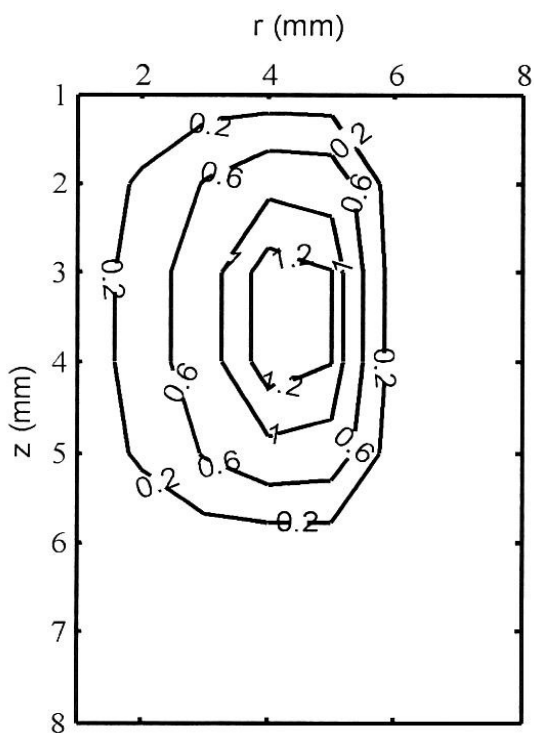
c. 0.5 sec
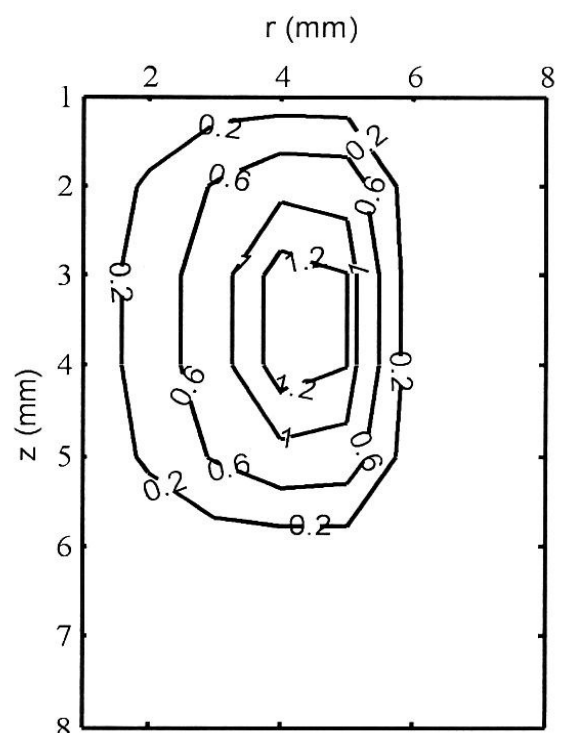
d. 0.75 sec

Fig.(6): Calculated Stream Function Contours in GMA Weld Pool at Different Times.

a. 0.1 sec

b. 0.3 sec

c. 0.5 sec

d. 0.75 sec
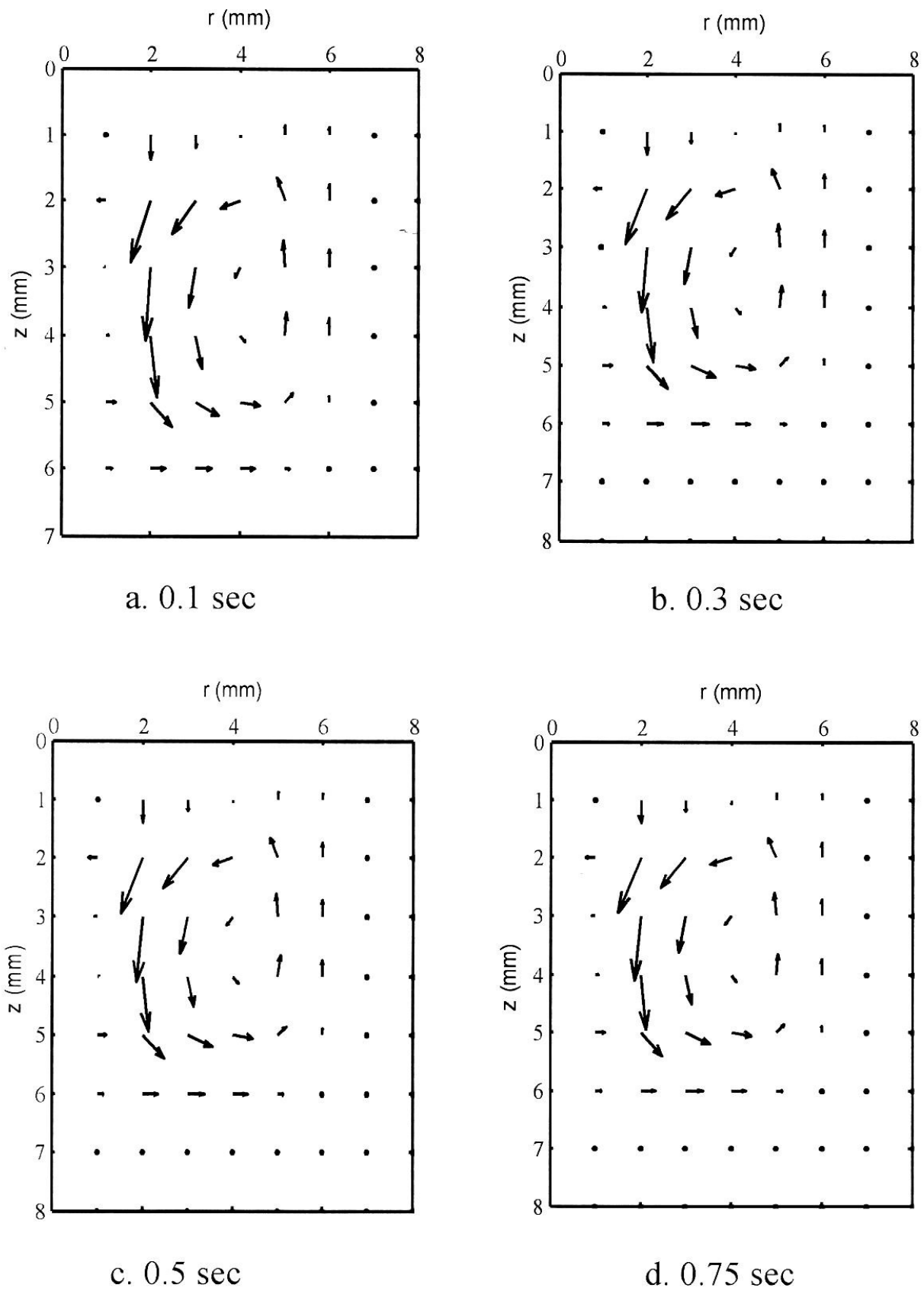
Fig.(7): Calculated Velocity Distribution in GMA Weld Pool at Different Times.
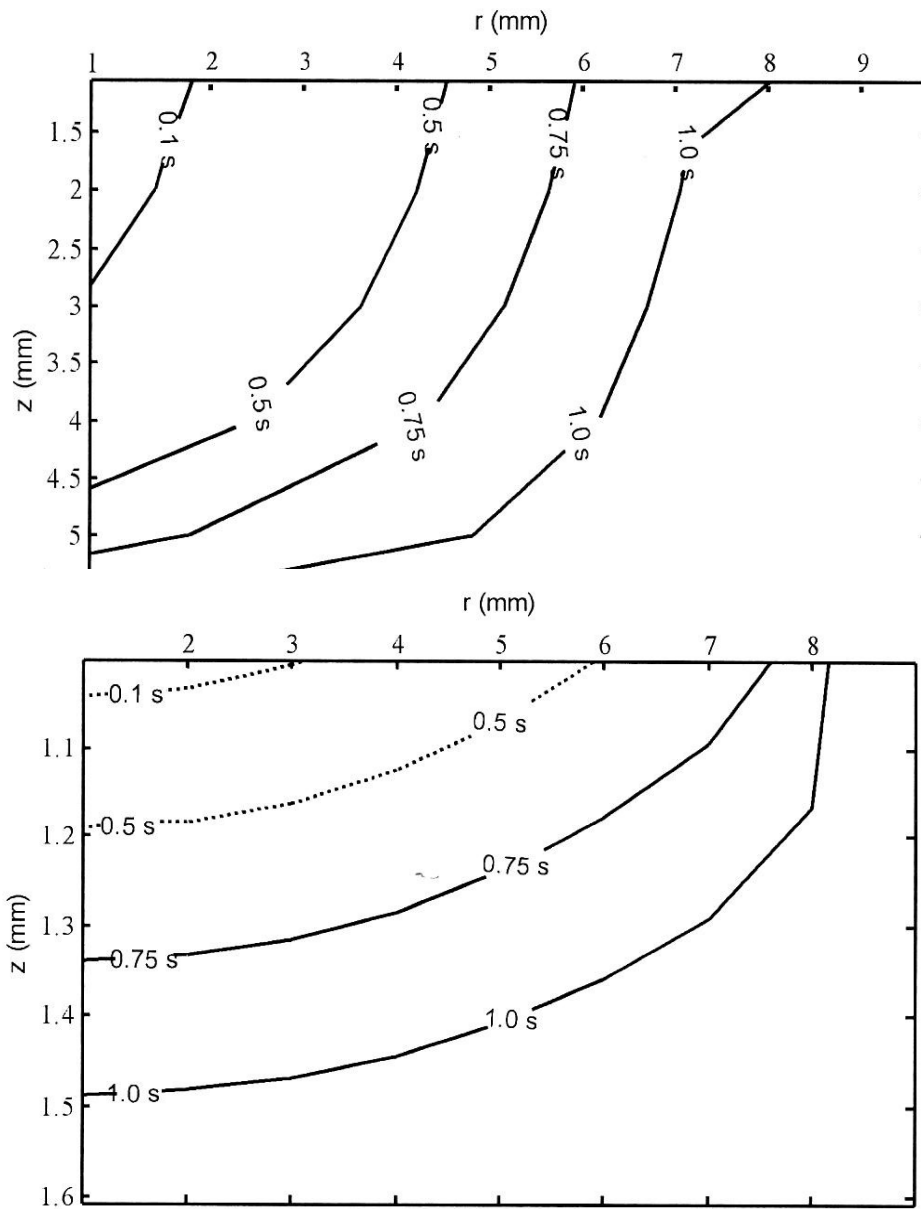
Fig.(9): Calculated Liquid – Solid interface of TIG Welding
With Same Heat Input at Different Times.
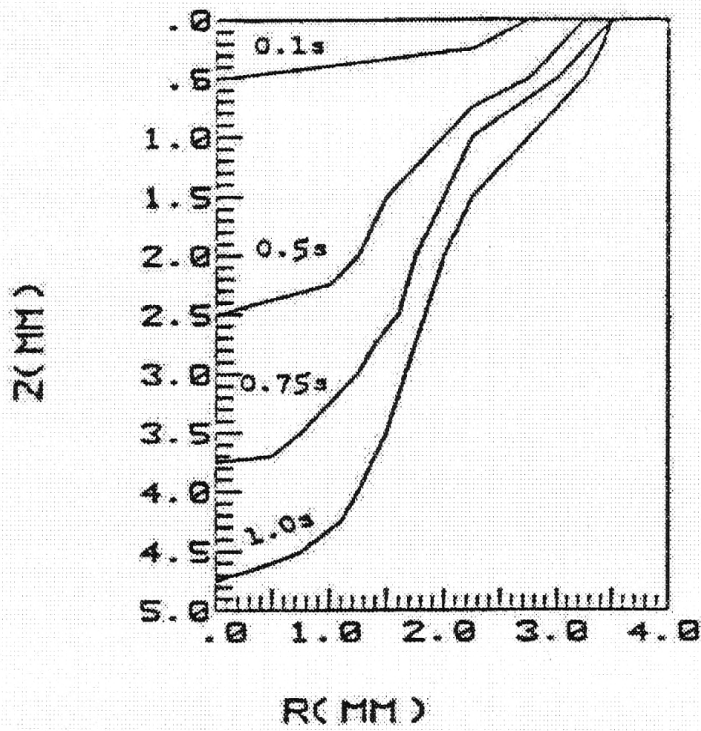
Fig.(10): Liquid – Solid Interface of GMA Welding
Ref.(Tsao and Wu 1988)
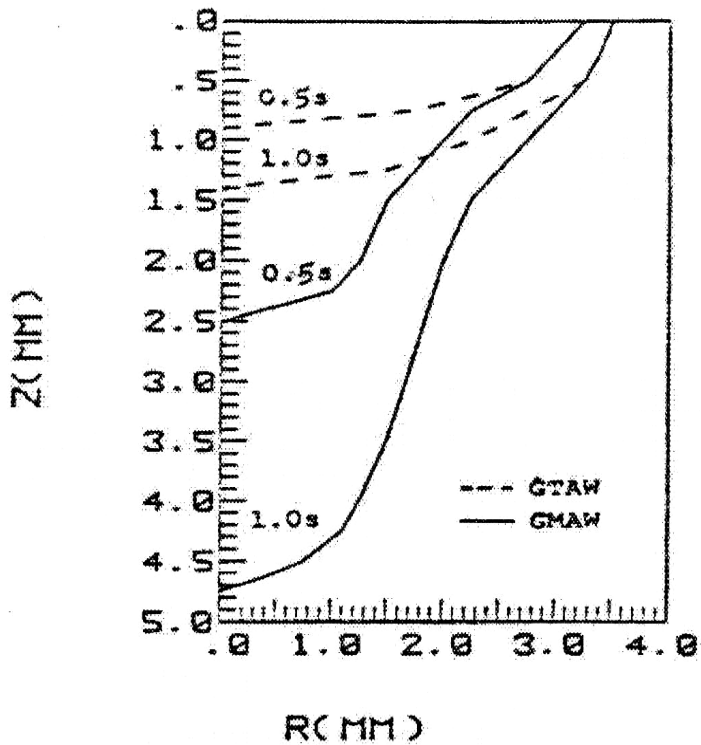
Fig.(11): Comparison of GMA and TIG weld Pool Boundaries
with the Same Heat Input Ref.(Tsao and Wu 1988)

REFERENCES

Chow, C. Y., "An Introduction to Fluid Mechanics", Wiley, New York, 1979.

Gukan, R., Guha, B. and Sundararajan, T., "Finite Element Modeling of Fluid Flow on Weld Pentration of Stationary Gas-Tungsten-Arc Weld Pool", Department of Mechanical Engineering – IIT Madras. Chemmai-600 036 , 2001, p.p. 279-285.

Kim, J. W. and Na, S. J., "A Study on The Three-Dimensional Analysis of Heat and Fluid Flow in Gas Metal Arc Welding Using Boundary-Fitted Coordinates", Journal of Engineering for Industry, Vol. 116, February 1994, p.p. 78-85.

Oreper, G. M. and Szekely, J., "A Comprehensive Representation of Transient Weld Pool Development in Spot Welding Operations", Metallurgical Transactions A, Vol. 18A, July 1987, p.p. 1325.

Petrovic, Z. and Stupper, S., "Computational Fluid Dynamics One", Mechanical Engineering Falculty, Belgrade, 1996.

Salah S. Abed-Alkreem , " Evaluation of Temperature Distribution and Fluid Flow in Fusion Welding Processes ", P.H.D Thesis, The College of Engineering , Mechanical Engineering Dept. ,University of Baghdad, March 2005.

Torrance, K. E., "Numerical Method in Heat Transfer", Handbook of Heat Transfer Fundamentals, McGraw-Hill, second edition, 1985.

Tsai, M. C. and Kou, S., "Electromagnetic Force Induced Convection in Weld Pools With A Free Surface", Welding Journal, Vol. 69, No. 6, June 1990, p.p. 241S-246S.

Tsao, K. C. and Wu, C. S., "Fluid Flow and Heat Transfer in GMA Weld Pools", Welding Journal, March 1988, p.p. 70S-75S.

NOMENCLATURE

Latin Symbols

Symbol	Definition	Unit
Co	Length scale factor if scale uses in mm=10^6	—
g	Acceleration of gravity	mm/sec^2
h	Convection heat transfer coefficient	J/mm^2. sec.°C
H	Length of plate	mm
i	Finite difference index in the r-direction	—
I	Welding current	Ampere
IFL	Index of fusion limit in r-direction.	—
j	Finite difference index in the z-direction	—
j(r)	Welding current distribution at the plane (z=0)	Amp/mm^2
JFL	Index of fusion limit in z-direction.	—
K_L	Thermal conductivity of liquid metal	W/mm.°C
K_s	Thermal conductivity of solid metal	W/mm.°C
L	Thickness of work piece	mm
M	Number of grid in z-direction	—

N	Number of grid in r-direction	—
N_r	Number of grid in r-direction of weld pool	—
N_z	Number of grid in z-direction of weld pool	—
$q(r)$	Heat flux on the plane at z=0	J/mm^2
Q	Heat input per unit time	W
r	Cylindrical coordinates.	mm
T	Temperature in x-y coordinates, also temperature of weldment.	°C
T_a	Ambient temperature	°C
T_i	Initial temperature	°C
T_m	Melting temperature	°C
T_s	Solid temperature	°C
U	Velocity in radial direction (r)	mm/sec
U_b	Average back velocity in r-direction	mm/sec
U_{b0}	Average back velocity at center line	mm/sec
U_f	Average front velocity in r-direction	mm/sec
U_{f0}	Average front velocity at center line	mm/sec
V	Velocity in axial direction (z)	mm/sec
V	Voltage duty	Volts
V_b	Average back velocity in z-direction	mm/sec
V_{b0}	Average back velocity at center line	mm/sec
V_f	Average front velocity in z-direction	mm/sec
V_{f0}	Average front velocity at center line	mm/sec
W	Width of plate also width of workpiece.	mm
z	Cylindrical coordinate	mm

GREEK SYMBOLS

Symbol	Definition	Unit
α_L	Thermal diffusivity of molten metal	mm^2/sec
α_S	Thermal diffusivity of solid metal	mm^2/sec
β	Coefficient of thermal expansion (exposivity)	1/k
ΔH	Heat transferred into weld pool by molten filler droplets	w/mm^{-3}
Δr	Step size in r-direction	mm
Δz	Step size in z-direction	mm
η	Heat input efficiency	—
μ	Dynamic viscosity	kg/mm.sec
μ_0	Magnetic permeability of free space	H/mm
υ	Kinematic viscosity	mm^2/sec
ρ_1	Density of welding wire	Kg/mm^3
ρ_2	Density of filler droplet	Kg/mm^3
σ	Surface tension	N/mm
σ_j	Current distribution parameter	Amp/mm^2
σ_q	Heat flux distribution parameter	w/mm^2
ψ	Stream function	M^3/sec
Ω	Successive over relaxation parameter	—
Ω_{OPT}	Optimum successive over relaxation parameter	—
ω	Vorticity	1/sec
ƒ	Spray transfer frequency	HZ